Laboratory Measurements of Axis Ratios for Large Raindrops

KAREN ANDSAGER, KENNETH V. BEARD,* AND NEIL F. LAIRD

Atmospheric Environment Section, Illinois State Water Survey, Champaign, Illinois

(Manuscript received 2 March 1998, in final form 16 October 1998)

ABSTRACT

The oscillations of moderate to large raindrops are investigated using a seven-story fall column with shape data obtained from multiple-strobe photographs. Measurements are made at a fall distance of 25 m for drops of $D = 2.5$-, 2.9-, 3.6-, and 4.0-mm diameter, with additional measurements at intermediate distances to assess the role of aerodynamic feedback as the source of drop oscillations. Oscillations, initiated by the drop generator, are found to decay during the first few meters of fall and then increase to where the drops attained terminal speed near 10 m. Throughout the lower half of the fall column, the oscillation amplitudes are essentially constant. These apparently steady-state oscillations are attributed to resonance with vortex shedding.

For $D = 2.5$ and 3.6 mm, the mean axis ratio is near the theoretical equilibrium value, a result consistent with axisymmetric (oblate/prolate mode) oscillations at the fundamental frequency. For $D = 2.9$ and 4.0 mm, however, the mean axis ratio is larger than the theoretical equilibrium value by 0.01 to 0.03, a characteristic of transverse mode oscillations. Comparison with previous axis ratio and vortex-shedding measurements suggests that the oscillation modes of raindrops are sensitive to initial conditions, but because of the prevalence of off-center drop collisions, the predominant steady-state response in rain is expected to be transverse mode oscillations.

A simple formula is obtained from laboratory and field measurements to account for the generally higher average axis ratio of raindrops having transverse mode oscillations. In the application to light to heavy rainfall, the ensemble mean axis ratios for raindrop sizes of $D = 1.5$–4.0 mm are shifted above equilibrium values by 0.01–0.04, as a result of steady-state transverse mode oscillations maintained intrinsically by vortex shedding. Compared to the previous axis ratio formula based on wind tunnel measurements, the increased axis ratios for oscillating raindrops amount to a reduction of 0.1–0.4 dB in radar differential reflectivity Z_{DR}, and an increase of about 0.5 mm for a reflectivity-weighted mean drop size of less than about 3 mm.

1. Introduction

The shape of raindrops is a critical factor in estimating rain intensity using advanced weather radars that transmit and/or receive pulses having orthogonal polarization. Because raindrops are aspherical, having a larger horizontal chord (h) than vertical chord (v), the radar reflectivity from a horizontally polarized pulse (Z_H) in rain will be larger than from a vertically polarized pulse (Z_V). Thus, the difference between these orthogonal reflectivities depends on the axis ratios of raindrops, $\alpha = v/h$.

In proposing the use of a differential radar reflectivity [Z_{DR}(dB) = 10 log(Z_H/Z_V)] to improve radar rainfall estimates, Seliga and Bringi (1976) relied on equilibrium axis ratios measured in a vertical wind tunnel by Pruppacher and Beard (1970), expressed as a linear function of the equivalent spherical diameter. Recent laboratory and field measurements, however, have shown that raindrops with diameters larger than $D = 1$ mm continuously oscillate in response to vortex shedding (Beard et al. 1989; Beard and Tokay 1991). Continuous oscillations were also found when the laboratory studies were extended to $D = 2.5$ mm (Kubesh and Beard 1993), and in more recent field measurements (Tokay and Beard 1996), continuous raindrop oscillations were found from $D = 1.0$ mm to $D = 4.0$ mm (the largest size measured). Aircraft measurements of raindrop shape for $D = 2$–6 mm also show large variations from equilibrium axis ratios (Chandrasekar et al. 1988).

Of particular significance to estimating rainfall rate using polarization radar is the observed shift in the time average axis ratio for oscillating raindrops. For example, the higher average axis ratios from laboratory measurements of Kubesh and Beard (1993) for $D = 2.0$ and 2.5 mm decrease the Z_{DR}(dB) signal for these sizes by about 30%. Evidence of a decrease in Z_{DR} has been found by comparing measurements of Z_{DR} with values calculated from raindrop size distributions measured be-

* Additional affiliation: Department of Atmospheric Sciences, University of Illinois, Urbana–Champaign, Urbana, Illinois.

Corresponding author address: Kenneth V. Beard, Department of Atmospheric Sciences, UIUC, 105 S. Gregory St., Urbana, IL 61801. E-mail: k-beard@uiuc.edu

TABLE 1. Experiment parameters for $D = 2.5$, 2.9, 3.6 and 4.0 mm: terminal velocity (V), Reynolds number at terminal velocity (Re), drop spacing (Δz) at terminal velocity (for drip rate of 2.3 Hz), distance to achieve 99% of terminal velocity (z_{99}), distance to reduce the oscillation amplitude to $\Delta\alpha = 0.01$ (z_{01}, as predicted by viscous decay), oscillation frequency for the fundamental mode (f_2), and number of oscillations at the fundamental frequency (ν_2) between z_{99} and the lowest measurement level at $z = 25.5$ m.

D (mm)	Re	V (m s^{-1})	Δz (m)	z_{99} (m)	z_{01} (m)	f_2 (Hz)	ν_2
2.5	1194	7.24	3.1	10.2	4.5	87.1	184
2.9	1489	7.78	3.4	11.2	7.4	69.7	128
3.6	2010	8.46	3.7	12.0	14.3	50.4	80
4.0	2303	8.72	3.8	12.1	19.2	43.0	66

low the radar pulse volumes (Goddard and Cherry 1984).

The purpose of the present experiment was to extend the previous laboratory measurements for moderate-size raindrops by Kubesh and Beard (1993) to larger sizes using the same 25.5-m fall column. In the previous study, drops of $D = 2.0$ and 2.5 mm were generated at terminal speed with a Reynolds number above the onset for vortex shedding (Re $= \rho DV/\eta \cong 300$, where ρ and η are the density and viscosity of air). The drops were therefore initially subjected to aerodynamic pressure fluctuations as well as large amplitude oscillations as result of drop generation. In the present study we generated drops from rest using a capillary ''dripper'' so that aerodynamic forcing would be initially negligible. Generating drops from rest also allowed more time for the initial oscillations to decay before measuring the axis ratio at fixed fall distance.

2. Experiment

a. Experimental parameters

The experimental parameters for the drop sizes investigated in our study are given in Table 1 for standard laboratory conditions of 20°C and a pressure of 1 atmosphere. The smallest size of $D = 2.5$ mm was chosen to be the same as the largest size studied by Kubesh and Beard (1993) to provide a comparison between the results for drops generated at rest and terminal speed. Ideally, the sizes would have been selected at 0.5-mm diameter intervals, but because of the limitation of capillary size the drops were produced at $D = 2.5$, 2.9, 3.6, and 4.0 mm.

The drop diameter (D) and terminal speed (V) in this study result in Reynolds numbers in the range 1200–2300, where the wake has an irregular vortex pattern as observed for spheres falling in liquids (see Beard et al. 1991). The vertical separation of successive drops (Δz) at terminal speed is calculated from the typical drop generation rate of 2.3 drops per second. At these wide separations of 1000 diameters there should be no appreciable aerodynamic influence between successive drops. According to the measurements of List and Hand (1971), for a drop with $D = 2.9$ mm falling at Re $\cong$ 1360, the disturbed airflow caused by the passage of the drop at a fixed level is surprisingly small: peak velocities of less than 2 cm s^{-1} immediately after passage and less than 1 cm^{-1} after (2.3 Hz)$^{-1} = 0.44$ s, the time between drop passages in the present experiment.

The calculated distance for a drop to reach 99% of its terminal velocity in Table 1 (z_{99}) includes the effect of increasing drag from a decreasing axis ratio as the drop accelerates (Beard 1977). The fall distance (z_{01}) was calculated for a drop to decay by viscous dissipation from its initial amplitude at the generator to a negligible amplitude of $\Delta\alpha = 0.01$. The oscillation amplitude was defined as the difference between the mean axis ratio ($\overline{\alpha}$) and the minimum value ($\alpha_{\min}$) at the point of maximum oblate distortion: $\Delta\alpha = \overline{\alpha} - \alpha_{\min}$. According to viscous decay theory, drops of all four sizes in the experiment fell through an appreciable portion of the fall column at terminal velocity with a surplus of time for damping out the initial oscillations, because the fall column of 25.5 m is significantly longer than z_{99} and z_{01}.

The last two parameters in Table 1 give the oscillation frequency of the fundamental mode (f_2) and the corresponding number of oscillation cycles (ν_2) as a drop falls from the height of z_{99} down to the lowest measurement section at $z = 25.5$ m. The large value of ν_2 demonstrates that there is sufficient time for oscillations to adjust after the drop has reached terminal speed and after the initial oscillation energy should have been mostly dissipated. Because the relaxation time for diffusion of momentum about a sphere is of order $\tau_s = 0.04\ D^2\rho/\eta$ (Bird et al. 1960), the airflow around a $D = 4$ mm drop can adjust for 1.8 time constants during one oscillation cycle of f_2. This indicates that the airflow around the drop can achieve a quasi-steady equilibrium with oscillating drops in the lower portion of the fall column. Because the oscillation frequency and decay rate increase for the harmonics of the fundamental mode, the values of z_{01} and ν_2 in Table 1 represent the maximum decay distance (z_{01}) and the minimum number of oscillation cycles ν_2.

b. Experimental design

The experiment was located in the stairwell of a six-story building and consisted of a drop generator at the penthouse level, a fall column extending down to the basement, and a camera section that could be placed at various levels in between (see Fig. 1). The fall column was assembled using a 46-cm-diameter ventilation duct having a helical wire frame. At each floor, a platform

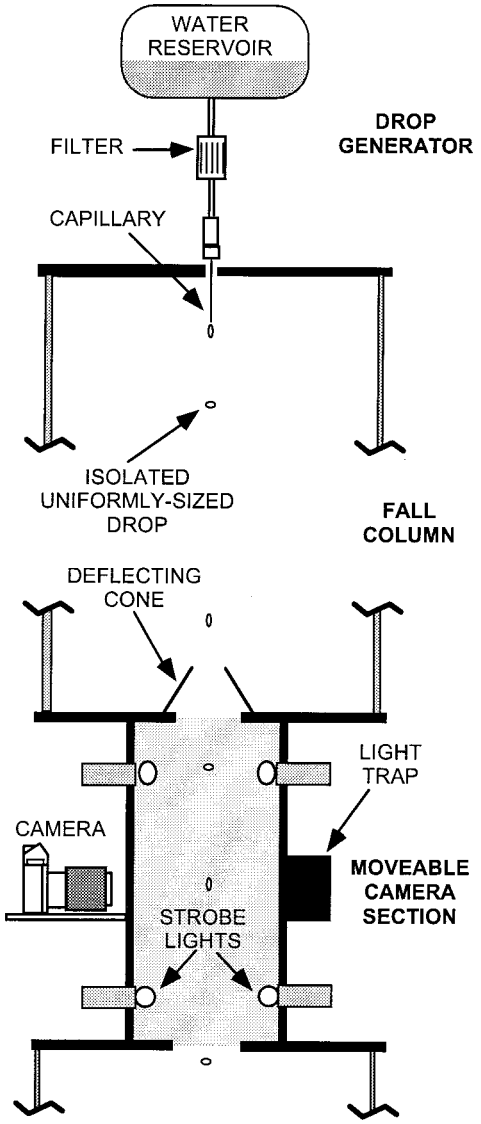

FIG. 1. Diagram of experiment showing drop generator, fall column, and camera unit. Drops were produced by dripping water from a stainless steel capillary with deionized water fed from an elevated reservoir through a filter. Drops falling through the center of the camera unit were photographed against a light trap using strobes to illuminate the surrounding interior. The camera unit could be positioned at any of seven levels to obtain data at fall distances up to 25.5 m.

was mounted over the opening between railings, and a duct section extended to the platform below. This design allowed the measurement section, containing the strobes and camera, to be placed on a platform at any floor by simply lifting the duct, inserting the camera section, and resting the duct on top.

The drop generator consisted of a stainless steel capillary supplied by a reservoir of deionized water. The drop size was controlled by the capillary bore size and drip rate was adjusted by changing the height of the water reservoir above the capillary tip. The relatively

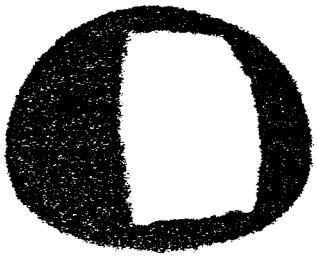

FIG. 2. Photographic negative image of 4.0-mm-diameter drop having an axis ratio of 0.80, approximately the mean axis ratio at fall distances of 10.1, 17.4, and 25.5 m. The light region in the center of the drop is the rectangular light trap directly behind the drop.

large horizontal cross section of the reservoir allowed the drip rate and drop size to remain essentially constant over the course of an experimental run of a few hours. Drop sizes, obtained by measuring the mass of individual drops, were consistent to within 1% over an individual experimental run and to within 2% between separate runs at one drop size.

Data on drop shape were collected by photographing the drops as they fell through the camera section (Fig. 1). Deflecting cones were used to isolate drops that fell within the camera viewing area. The drops were illuminated by four synchronized strobes placed just within the 15-cm diameter camera column. An example image of a 4-mm diameter drop is shown in Fig. 2. Because a clear water drop acts as a lens, the light trap appears as a white distorted rectangle on the negative image. Drop images of ¼ true size on the film were taken using a 35-mm camera equipped with a 50-mm lens and power winder. The combination of available strobe lighting and film speed allowed two to three images per drop to be recorded on one frame of film for those fall distances where the drops were moving at terminal speed (z = 10–25.5 m). These multiple images allowed for multiple axis ratio measurements of the same drop.

Because of poor insulation in the stairwell, the temperature ranged from a low of 8°C in the winter to a high of 28°C in the summer. Over this temperature range, the fall speeds change by only 3% (Table 2; Beard and Heymsfield 1988) and the surface tension changes by only 1%. Also, the oscillation frequency, which depends on the square roots of drop volume, water density, and surface tension, is affected by less than 1%. Appreciable changes in water viscosity over the 21°C temperature range resulted in a +20% to −27% change in the decay time constant from the values in Table 1 at 20°C. Therefore, the effect of temperature is negligible for all the experimental parameters in Table 1, except for the theoretical damping distance (z_{01}).

3. Data analysis

Axis ratios were obtained by measuring the maximum vertical and horizontal chords (v, h) from the negative image of each drop using a microscope with a micro-

TABLE 2. Parameters for the 26 experiment runs at four drop diameters tabulated by drop diameter–run number (expt), fall distance to camera (z), number of axis ratio measurements (N), mean axis ratio ($\overline{\alpha}$), standard deviation (σ), 95% confidence interval for the estimate of the mean [95% confidence interval (CI)], minimum axis ratio (α_{min}), and maximum axis ratio (α_{max}).

Expt	z (m)	N	$\overline{\alpha}$	σ	95% CI	α_{min}	α_{max}
2.5–1	0.65	143	0.975	0.024	0.004	0.915	1.090
2.5–2	2.8	265	0.928	0.018	0.002	0.879	0.994
2.5–3	10.1	265	0.887	0.023	0.002	0.804	0.967
2.5–4	25.5	117	0.892	0.019	0.004	0.846	0.944
2.9–1	25.5	103	0.874	0.029	0.006	0.812	0.947
3.6–1 to 2	25.5	210	0.798	0.036	0.005	0.704	0.899
4.0–1 to 4	0.65	299	0.979	0.084	0.010	0.824	1.178
4.0–5 to 8	2.8	660	0.880	0.025	0.002	0.811	0.957
4.0–9 to 10	6.5	345	0.818	0.041	0.004	0.718	0.958
4.0–11 to 13	10.1	485	0.796	0.046	0.004	0.633	0.933
4.0–14 to 16	21	337	0.796	0.043	0.005	0.663	0.934
4.0–17 to 19	25.5	326	0.808	0.045	0.005	0.691	0.928

meter eyepiece. A plumb line was placed in the camera section and photographed before each experimental run. This negative was used to align each drop image before measuring the maximum vertical and horizontal chords. The uncertainty in axis ratio measurements was estimated to be $\delta\alpha = \pm 0.01$, based on repeated measurement of drop images.

Data were obtained at the greatest fall distance (25.5 m) for four drop sizes: $D = 2.5$, 2.9, 3.6, and 4.0 mm. Data were also obtained at the intermediate levels of 6.3 and 10.1 m for $D = 2.5$ and 4.0 mm, with additional measurements at 21.1 m for $D = 4.0$ mm. Also, for $D = 4.0$ mm, data were collected at upper levels, before the drops reached terminal velocity. Additional experimental runs were made to check the consistency of the measured axis ratios.

Table 2 contains summary information on the axis ratio measurements for the four drop diameters. This information is grouped by drop diameter with results combined at each fall distance. There were no significant differences among experimental runs taken at the same fall distance for a given drop size. Table 2 includes the fall distance (z) and number of axis ratio measurements (N), as well as the mean axis ratio ($\overline{\alpha}$), standard deviation (σ), 95% confidence interval for the estimate of the mean (95% CI), maximum axis ratio (α_{max}), and minimum axis ratio (α_{min}).

Drop images for $D = 4.0$ mm were recorded just below the dripper at about a dozen different fall distances (in the range $z = 0.60$–0.70 m) to obtain representative axis ratios for a complete oscillation cycle, and for use as an ''initial'' amplitude in calculating viscous decay. Analysis of these images indicated large amplitude oblate–prolate oscillations. The oscillations of successive drops appeared to be in phase at the same distance (z) below the capillary during a single experimental run. The drops were generally much less in phase after falling to $z = 2.8$ m, and there was no indication of oscillations being in phase at lower levels ($z \geq 6.5$ m).

4. Results

a. Oscillation behavior at different fall distances

Measurements were made at several levels for $D = 2.5$ and 4.0 mm to examine the decay of oscillations induced by the dripper and the change in mean axis ratio with fall distance. For $D = 2.5$ mm, the initial mean axis ratio was found to decrease between levels at $z = 0.65$, 2.8, and 10.1 m and then remain essentially constant to $z = 25.5$ m, where $\alpha = 0.89$ (see Table 2). Judging from relatively constant standard deviations (0.018–0.024), the axis ratio amplitude for $D = 2.5$ mm does not appear to change appreciably during the drop's fall.

For $D = 4.0$ mm, the initial mean axis ratio was found to decrease between successive levels at $z = 0.65$, 2.8, 6.5, and 10.1 m, and then remain essentially constant to the lowest level, where $\alpha = 0.81$ (see Table 2). The standard deviations of 0.03–0.07 indicate that the axis ratio amplitude for $D = 4.0$ mm decayed substantially from $z = 0.65$ to 2.5 m, increased at $z = 6.5$ m and 10.1 m, and then remained nearly constant to the lowest level at $z = 25.5$ m. The axis ratio data for $D = 4.0$ mm from experimental runs at the six fall distances are plotted in Fig. 3 for comparison with calculations of oscillation damping. The axis ratios at each level are represented by a ''box'' having a center bar at the mean ($\overline{\alpha}$) and the top and bottom of the box at the 95% confidence interval about the mean. The bent error bars show the range of the standard deviation about the mean axis ratio ($\overline{\alpha} \pm \sigma$), and the straight bars denote the extremes (α_{max}, α_{min}).

Oscillation amplitudes were estimated from the data using values of α_{max} and α_{min}, which are given in Table 2 and plotted by vertical bars in Fig. 3. For example, the range in axis ratio for $D = 4.0$ mm observed at $z = 0.65$ m is $\alpha_{max} - \alpha_{min} = 0.354$. Therefore, the amplitude for a sinusoidal oscillation would be $\Delta\alpha = 0.345/2 = 0.177$. Sinusoidal amplitudes are consistent

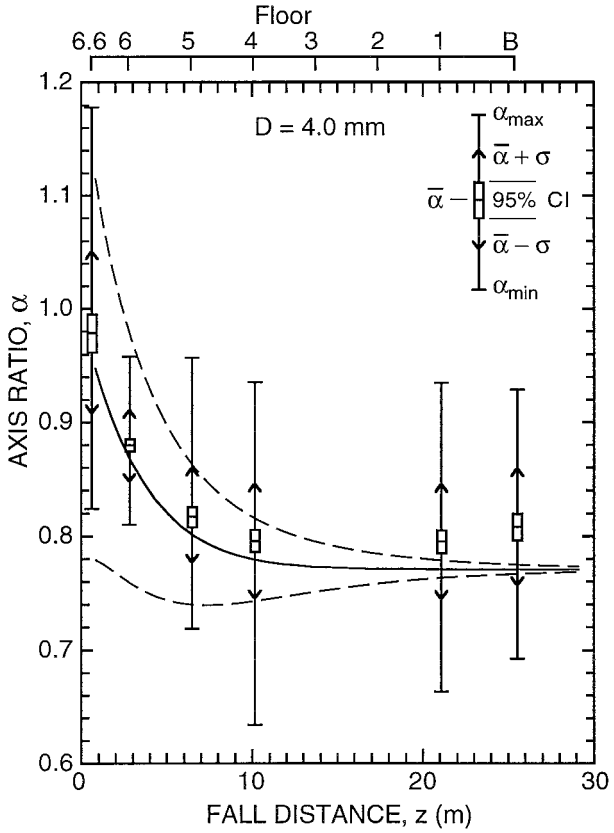

FIG. 3. Axis ratio parameters for $D = 4.0$ mm averaged for measurements at each fall distance: $z = 0.65$, 2.8, 6.5, 10.1, 21.1, and 25.5 m (at ''floors'' labeled 6.6, 6, 5, 4, 1, and B). Plotted at each level are values for the mean axis ratio, the 95% confidence interval for the mean, the range for the standard deviation, and the maximum and minimum axis ratios (see key in upper-right corner). The solid curve shows the theoretical axis ratio change for a nonoscillating 4-mm drop accelerating from rest. The dashed curves show the axis ratio envelope for viscous decay.

with oscillations of the spheroidal mode (see Beard 1984).

In Fig. 3, the solid curve is the axis ratio calculated from an oblate distortion response to the change in hydrostatic pressure for a 4-mm drop accelerating from rest (Beard 1977). In this hydrostatic model, an initially spherical drop becomes increasingly distorted as it accelerates, approaching its equilibrium axis ratio ($\alpha_H = 0.77$) at terminal speed. As shown in Table 1, 99% of terminal speed is attained at $z_{99} = 12.1$ m, where the axis ratio becomes essentially constant (see Fig. 3). At a fall distance of 2.8 m, the initial oscillations for $D = 4.0$ mm damp to where the standard deviation was the smallest of any level ($\sigma = 0.03$) and the Reynolds number was larger than 300, indicating that vortex shedding should have been present. At the 6.5-m fall distance, the standard deviation of the axis ratios increased back to about 0.04, and at greater fall distances the standard deviations were typically 0.04–0.05. From these axis ratio results in Fig. 3 it is readily apparent that some mechanism, other than the initial oscillations produced by the drop generator, is 1) causing oscillations as the 4-mm drops approach terminal speed and 2) maintaining oscillations thereafter at a nearly constant amplitude.

The dashed curves in Fig. 3 delineate an amplitude envelope for viscous decay obtained from a time constant for the fundamental mode oscillation: $\tau_2 = \rho_w D^2/(20\eta_w)$ (Pruppacher and Klett 1997). An initial amplitude of $\Delta\alpha = 0.26$ was chosen so that the decay would agree with the estimate from the measurements of $\Delta\alpha = 0.177$ at $z = 0.65$ m. For $D = 4.0$ mm, the time constant of $\tau_2 = 0.8$ s is much shorter than the 3.5-s fall time in this study. A reduction to $\Delta\alpha \simeq 0.01$ is predicted to occur at $z_{01} = 19$ m by viscous dissipation theory at 20°C, as is evident from the dashed curves in Fig. 3. Over the temperature range of the experiments (8°–28°C), $z_{01} = 13$–23 m because of changes in water viscosity with temperature.

From $z = 0.65$–2.8 m the observed decay was actually stronger than predicted by viscous dissipation of fundamental mode oscillations. Two mechanisms that would increase damping are vorticity diffusion and the stronger damping of higher harmonic oscillations. The latter would be induced as a drop releases from the dripper, because the drip shape is not a pure spherical harmonic. The more rapid decay of higher harmonics is evident from the time constants for $n = 3$ and 4, which are $(5/14)\tau_2$ and $(5/27)\tau_2$. The theoretical decay can be forced to agree with the observations at both $z = 0.65$ and 2.8 m by using a decay time constant of $0.55\tau_2$ and increasing the initial amplitude at $z = 0$ to $\Delta\alpha = 0.35$. The factor $0.55\tau_2$ therefore represents an effective decay time constant for an assumed exponential decay of oscillation energy in the first few meters of fall. The additional damping is probably caused by vorticity diffusion because of the circulation generated in the large amplitude oscillations (Prosperetti 1977).

Despite the strong damping observed for the initial oscillations for $D = 4.0$ mm, the oscillation amplitudes increase from $z = 2.8$ to 10.1 m. The oscillation amplitudes exceed the envelope for viscous dissipation beyond about 5 m and during the final 80% of its fall distance and 70% of its fall time.

b. Axis ratios at the maximum fall distance

The distributions and means for our axis ratio measurements at the maximum fall distance of $z = 25.5$ m are presented in Fig. 4. For each drop size the distribution of axis ratios is a histogram having a horizontal scale for the number of observations in each 0.01 interval of axis ratio. The shaded region in Fig. 4 indicates the range of the equilibrium axis ratio from previous estimates given in Table 3. Our mean axis ratio ($\overline{\alpha}$, indicated by arrows) is within the range of equilibrium axis ratio for $D = 2.5$ and 3.6 mm, but above the range for $D = 2.9$ and 4.0 mm.

Our data have standard deviations of 0.019–0.045

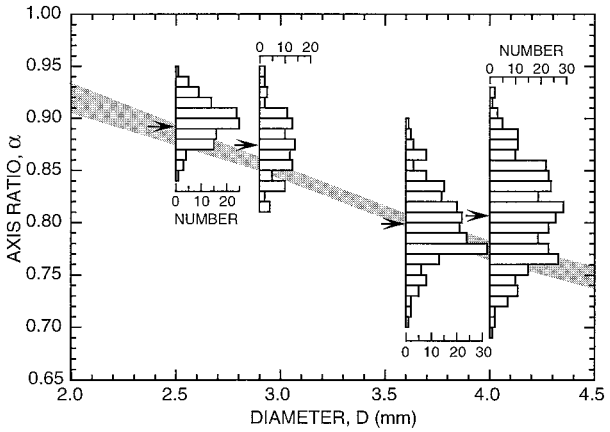

FIG. 4. Measured axis ratios for $D = 2.5$, 2.9, 3.6, and 4.0 mm at a fall distance of $z = 25.5$ m. Distributions are shown for each drop size with mean axis ratios indicated by arrows. The shaded region covers the range for previous estimates of the equilibrium axis ratio (see Table 3).

(Table 2), which is much larger than the experimental uncertainty of 0.01, whereas the 95% confidence intervals for the means are smaller ($\approx$0.005, Table 2). Thus, the histograms in Fig. 4 appear to provide reasonable estimates of the mean and variance of axis ratios for water drops falling at terminal velocity.

The distributions of axis ratios have a range of ± 0.05 to ± 0.10 with either a distinct central peak for $D = 2.5$ and 3.6 mm, or a broad central maximum for $D = 2.9$ and 4.0 mm. Axis ratios obtained from a drop oscillating with a constant amplitude would result in a secant distribution having a central minimum with peaks at the maximum and minimum axis ratios, because the changes in axis ratio are slowest at the turning points where the axis ratios have extreme values.

A simple interpretation of the distributions in Fig. 4 is that the axis ratios were obtained for drops oscillating with a variety of amplitudes—more with low amplitudes than high amplitudes, so that their sum has a central maximum [for particular examples, see Kubesh (1991)]. This interpretation was suggested by Chandrasekar et al. (1988) based on aircraft observations of raindrop axis ratios. The oscillation modes cannot be easily deduced from these distributions, because of the likely occurrence of various axis ratio amplitudes. However, when a mean axis ratio differs significantly from the equilibrium (nonoscillating) value, this information may be used to infer particular oscillation modes [e.g., as discussed in Beard and Kubesh (1991)].

5. Discussion

a. Comparison with previous results

Mean axis ratios ($\overline{\alpha}$) at $z = 25.5$ m are tabulated in Table 3 for comparison with equilibrium axis ratios from past research: α_W, the linear fit to wind tunnel data by Pruppacher and Beard (1970); α_P, the perturbation model of Pruppacher and Pitter (1971); α_H, the hydrostatic model of Green (1975); and α_N, the numerical model (Beard and Chuang 1987). The range for previous equilibrium axis ratios, shown in the last column ($\Delta\alpha$) and extended from $D = 2.0$ to 4.5 mm, is represented by the shaded area in Fig. 4. The mean axis ratios from the present study ($\overline{\alpha}$) are within the range of previous axis ratios for $D = 2.5$ and 3.6, but our means are higher than previous values for $D = 2.9$ and 4.0 mm. These latter differences appear to be real because by comparison to the shaded region in Fig. 4, the means at $D = 2.9$ and 4.0 mm are displaced more than the 95% confidence interval above the range from previous studies.

TABLE 3. Experimental mean axis ratios ($\overline{\alpha}$) for each drop size at the maximum fall distance of $z = 25.5$ m in comparison to the emperical formula (α_W) from the wind tunnel study of Pruppacher and Beard (1970) and the equilibrium axis ratios from the perturbation model (α_P) of Pruppacher and Pitter (1971), the hydrostatic model (α_H) of Green (1975), and the numerical model (α_N) of Beard and Chuang (1987). Also shown is range in equilibrium axis ratios ($\Delta\alpha$) from previous research.

D (m)	$\overline{\alpha}$	α_W	α_P	α_H	α_N	$\Delta\alpha$
2.5	0.892	0.875	0.893	0.881	0.892	0.018
2.9	0.874	0.850	0.858	0.851	0.861	0.008
3.6	0.798	0.807	0.797	0.799	0.808	0.011
4.0	0.807	0.782	0.765	0.770	0.778	0.017

Axis ratio data for water drops falling at terminal velocity in air are presented in Fig. 5 for comparison with results from laboratory measurements, aircraft measurements, and theory. The curve for the equilibrium axis ratio (α_N) is from the numerical model of Beard and Chuang (1987). This theoretical result is in good agreement with average axis ratios from wind tunnel observations of drops in air [see Figs. 10–16, Pruppacher and Klett (1997)] and can be represented by

$$\alpha_N = 1.0048 + 0.0057D - 2.628D^2 + 3.682D^3 - 1.677D^4 \quad (1)$$

with diameter in units of centimeters. This formula is preferred to the one in Pruppacher and Klett (1997), which is based on the numerical results of Chuang and Beard (1990) for electrified raindrops, because more accurate terminal fall speeds could be used in the absence of electric forces. Note also that the formula for axis ratio in Pruppacher and Klett (1997) has a mistake: the first coefficient should be 1.016 68 rather than 1.101 668. Equation (1) provides axis ratios that deviate less than 0.003 from the numerical results over the range in D from 0 to 7 mm. Wind tunnel data typically scatter by about ± 0.015 above and below the mean axis ratio provided by (1).

Also shown in Fig. 5 is the dashed line from the empirical formula based on wind tunnel measurements of Pruppacher and Beard (1970):

$$\alpha_W = 1.030 - 0.62D \quad (2)$$

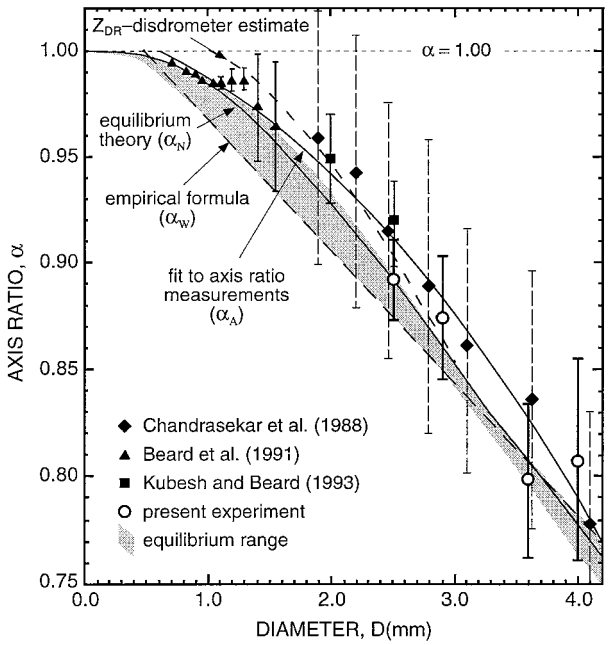

FIG. 5. Raindrop axis ratios as a function of diameter. Shown are mean axis ratios (symbols) and standard deviations (vertical lines) for the aircraft observations of Chandrasekar et al. (diamonds), the laboratory measurements of Beard et al. (triangles), Kubesh and Beard (squares), and present experiment (circles). Curves are shown for the numerical equilibrium axis ratio (α_N) from Beard and Chuang (1987), the radar–disdrometer-derived axis ratios of Goddard and Cherry (1984), the empirical formula (α_W) from the wind tunnel data of Pruppacher and Beard (1970), and the present fit to axis ratio measurements (α_A). The shaded region covers the range for previous estimates of the equilibrium axis ratio (see Table 3).

with diameter in units of centimeters. This early expression for axis ratio was used by Seliga and Bringi (1976) in their original paper on Z_{DR}. The dashed curve in Fig. 5 (labeled "Z_{DR}–disdrometer estimate") was obtained by Goddard and Cherry (1984) measurements of Z_{DR} with values calculated from corresponding disdrometer-obtained drop size distributions. The difference between the empirical formula of Pruppacher and Beard (α_W) and the dash curve is significant. For example, at $D = 2$ mm, the Z_{DR}–disdrometer estimate of axis ratio is $\alpha = 0.95$, whereas the result from the empirical formula is $\alpha_W = 0.90$. Thus, in rainfall characterized by a reflectivity-weighted mean diameter of 2 mm, the expected Z_{DR} signal using the Z_{DR}–disdrometer estimate is only half that of signal predicted by the empirical formula. This example demonstrates that such large differences in raindrop axis ratio need to be resolved.

The experimental axis ratios, shown in Fig. 5 for laboratory and aircraft measurements for oscillating drops, scatter about the equilibrium axis ratios (e.g., α_N) with means mostly above equilibrium for $D > 1$ mm. The shift in the mean above equilibrium axis ratio can be explained by transverse mode oscillations induced by vortex shedding, whereas the two-sided scatter can occur if a small fraction of the oscillation energy (<2%) excites the axisymmetric "spheroid" mode at the fundamental frequency (see Beard and Kubesh 1991; Kubesh and Beard 1993).

In laboratory measurements, Beard et al. (1989, 1991) determined from axis ratio scatter and optical measurements that water drops begin oscillating at 1-mm diameter, at the same size for the onset of vortex shedding. The threshold of 1-mm diameter for raindrop oscillation was documented in field measurements at the ground by Beard and Tokay (1991). As can be seen from Fig. 5, the laboratory studies also reveal that the mean axis ratios for $D > 1$ mm *are* larger than values for the corresponding equilibrium axis ratios.

For laboratory measurement of larger drop sizes of $D = 2.0$ and 2.5 mm, Kubesh and Beard (1993) also found that drops oscillated and had mean axis ratios that were higher than equilibrium values. Chandrasekar et al. (1988) in aircraft measurements of drops from $D =$ 2 to 3.6 mm also determined that the mean axis ratios were higher than equilibrium values.

The general trend for laboratory measurements in the range $D = 1.0$–2.5 mm is that the mean axis ratios are shifted above the equilibrium axis ratios in the direction suggested by Goddard and Cherry (1984) from Z_{DR}–disdrometer measurements (dashed curve).

In the present study the mean axis ratios for $D = 2.5$ and 3.6 mm were within the range of equilibrium values, whereas Kubesh and Beard (1993) obtained a mean axis ratio for $D = 2.5$ mm that was significantly above the equilibrium value. The standard deviations from these two studies are similar, indicating that the amplitude of the oscillations would be similar for similar oscillation modes. For $D = 2.9$ and 4.0 mm, our mean axis ratios are considerably above the range for equilibrium axis ratios, as are the mean axis ratios from the aircraft measurements of Chandrasekar et al. (1988). The aircraft data show considerably more fluctuation in axis ratio than laboratory data, possibly indicating that the axis ratios were broadened by turbulent fluctuations in the drop velocities (see Chandrasekar et al. 1988).

The laboratory results in Fig. 5 indicate that the oscillation amplitude, as characterized by the standard deviation, increases with drop size. This trend is consistent with the increase in the Weber number, the ratio of the aerodynamic perturbation force to the surface tension: $\mathrm{We} = \rho D v^2/\gamma$, where ρ is the air density, γ is the surface tension, and v is a perturbation velocity induced by vortex shedding. Note that the Weber number increases with drop size, even if the perturbation velocity remains constant. Therefore, oscillation amplitudes induced by vortex shedding should increase with drop size, as long as the forcing and response are suitably matched in both mode and frequency.

Axis ratio data from various wind tunnel studies [see Figs. 10–16, Pruppacher and Klett (1997)] agree with equilibrium axis ratios in the mean because they scatter only about ± 0.03 from theory (α_N). This is consistent with axisymmetric oscillations of small to moderate am-

plitude. The axis ratios for more strongly oscillating drops in Fig. 5, however, scatter mostly above theory. The differences in average axis ratios between wind tunnel measurements and those from laboratory and aircraft measurements may be due to different steady-state behaviors as a result of different initial conditions or different airflows.

b. Adequacy of simulations

In all previous measurements of raindrop shape, the environment has been altered to some degree from conditions in natural rain. The shape and oscillations of water drops suspended by the airstream in a vertical wind tunnel can be affected by turbulence and gradients in airflow used to keep the drops centered on the tunnel axis. Because of solid surfaces bounding, turning, and filtering the airflow, the intensity of wind tunnel turbulence and shear at the small scales affecting drop shape is much greater than in the atmosphere. Aircraft measurements of raindrop axis ratio can be affected by the accelerated airflow ahead of the sampling instrument (Beard 1983; Xu 1995), and there is uncertainty in the vertical dimension of raindrops because of fluctuations in vertical air velocity (Chandrasekar et al. 1988). Raindrop axis ratios at the ground can be altered by strong shear, although in light to moderate winds the influence of shear is probably negligible (Tokay and Beard 1996). Because natural turbulence in rain shafts above the ground and in clouds is probably too weak at the smaller scales needed to affect raindrop shape and oscillations (Tokay and Beard 1996), laboratory measurements of axis ratios in still air provide the best simulation of the raindrop environment. Here we note that the shape of raindrops falling aloft does not change appreciably from that at the surface (Beard 1976), because the distortion parameter (We) and the drag force are both proportional to the air density times the velocity squared. As the air density decreases aloft, the fall speed increases by an amount nearly proportional to the square root of density ratio. Thus, the distortion and drag forces do not change significantly with altitude for a fixed drop size (weight).

Additional requirements for simulating raindrop oscillations in the laboratory are 1) the damping of oscillations caused by the drop generator and 2) the attainment of steady-state oscillations in response to vortex shedding at terminal velocity. In our present experiment and earlier studies these requirements were achieved by using fall columns of sufficient height to allow the initial oscillations to decay and to permit a large number of oscillation cycles at terminal velocity before the axis ratios were measured.

Although the present study and that of Kubesh and Beard (1993) met the requirements for studying steady-state oscillations, two different oscillation behaviors were observed for $D = 2.5$ mm. Kubesh and Beard produced drops at terminal speed that reached a steady-state amplitude with axis ratios that scattered both above and below the equilibrium value. The mean axis ratio was greater by about 0.03 than equilibrium ratio. The initial conditions provided immediate aerodynamic feedback to drops oscillating at large amplitude ($\Delta\alpha \approx 0.3$). Kubesh and Beard attributed the more symmetric distribution of axis ratios at their highest measurement level to the presence of axisymmetric oscillations, and the more skewed distributions at the lowest measurements level to transverse mode oscillation in modes in response to asymmetric (transverse) vortex shedding. They suggested that because vortex shedding is an instability phenomenon, vortices may be triggered at suitable oscillation frequencies and modes. This sort of lock-in resonance has been observed for other systems, for example, elastically mounted cylinders in laminar cross flow (Mihailovic et al. 1997).

In the present study, steady-state oscillations for $D = 2.5$ and 3.6 mm showed two-sided scatter, as would be produced by axisymmetric oscillations. The absence of one-sided scatter was verified by an additional set of axis ratio measurements at 10.1 m for $D = 2.5$ mm and at 25.5 m for 3.6 mm (see Table 2). The oscillations caused by the drop generator were *predominantly* axisymmetric and only partially dissipated before the drops had achieved a sufficient speed for vortex shedding. As the drops accelerated, axisymmetric oscillations may have initiated axisymmetric vortices as observed by Winnikow and Chao (1966), thus providing a good match between the axisymmetric forcing and response in the steady state.

Because we observed a steady-state axis ratio behavior for $D = 2.5$ and 3.6 mm that was dominated by axisymmetric oscillations having a mean similar to equilibrium axis ratios, whereas Kubesh and Beard (1993) found a steady-state axis ratio behavior for $D = 2.0$ and 2.5 mm consistent with the axis ratio shift from transverse mode oscillations, it appears that oscillation modes in the steady state can be affected by initial conditions. The different outcomes can be attributed to differences in drop generators used in the two experiments: 1) symmetric oscillations produced by the dripper in the present experiment leading to axisymmetric mode oscillations in the steady state and 2) asymmetric oscillations during jet breakup in the experiment of Kubesh and Beard leading to transverse mode oscillations in the steady state.

If the above explanation is correct, then why did we observe the transverse mode behavior for $D = 2.9$ and 4.0 mm? Apparently, the transverse mode oscillations dominated the steady state, despite the axisymmetric initial conditions. This outcome may result from a better match between the oscillation frequency and the shedding of transverse vortices, for example, as a lock-in resonance. For $D = 2.9$ and 4.0 the steady-state oscillations appear to be insensitive to initial conditions.

Over the range in drop sizes in Fig. 5 from $D = 1.3$ to 4.0 mm, a scatter was found in axis ratios both above and below equilibrium values. This behavior is readily explained by axisymmetric oscillations, which require an order of magnitude less energy than the transverse

mode oscillations for the observed axis ratio amplitudes of $\Delta\alpha \leq 0.1$. The data in Fig. 5 also indicate that average axis ratios are usually larger than equilibrium values for $D = 1$–4 mm. The most likely mechanism for this behavior is vortex shedding that excites transverse mode oscillations with significantly larger oscillation energies than the axisymmetric mode.

c. Drop collisions in rain

The growth of raindrops in the warm rain process occurs primarily by the collection of cloud drops. The excess energy for the inelastic collisions (i.e., coalescences) between raindrops and cloud drops is many orders of magnitude less than the surface energy of a raindrop, so the resultant oscillations are negligible. In contrast, the occasional collision of a raindrop with a drizzle drop or smaller raindrop results in rapidly damped large-amplitude oscillations of coalesced pairs, or if energetic enough, breakup (see Beard et al. 1983).

Because collisions between precipitation drops are generally off center, they typically produce initial conditions similar to the experiment of Kubesh and Beard (1993), where jet breakup caused asymmetric oscillations in drops moving at sufficient speed for vortex shedding. The oscillations induced by off-center collisions should decay to a negligible amplitude within about 10 m of fall, as the steady-state oscillations in the transverse modes develop their characteristic shift in the mean axis ratio. This oscillation behavior was found by Kubesh and Beard for $D = 2.0$ and 2.5 mm. Our laboratory measurements with drops produced by axisymmetric initial conditions without immediate vortex shedding resulted in two types of steady-state oscillation behavior: significant transverse mode oscillations with a shift in mean axis ratio for $D = 2.9$ and 4.0 mm, but only axisymmetric mode oscillations for $D = 2.5$ and 3.6 mm. In rain, however, the more prevalent off-center collisions would initiate transverse mode oscillations for all raindrop sizes from $D = 1.0$–4.0 mm, which are maintained intrinsically in a steady state by vortex shedding.

In light to heavy rainfall, when the time between collisions is much longer than the oscillation decay time (Johnson and Beard 1984), the ensemble mean axis ratio should be dominated by steady-state oscillations having a mean axis ratio greater than the equilibrium axis ratio from oscillations in transverse modes, and a two-sided scatter about the equilibrium axis ratio from lower-energy oscillations in the axisymmetric mode. The laboratory results in Fig. 5 indicate that raindrops should oscillate with a standard deviation in axis ratio of $\sigma \approx 0.02$–0.03 in the intervals between raindrop collisions. The axis ratio shift should be about 0.01–0.03 for steady-state transverse mode oscillations initiated by collisions. In very heavy rainfall, the larger amplitude oscillations from more frequent collisions may dominate the steady-state oscillations and result in axis ratio shifts exceeding 0.03 (Jones 1959; Jameson and Beard 1982; Jameson 1983; Beard and Johnson 1984).

d. Average axis ratio formula

The average axis ratio can be represented by the curve labeled ''fit to axis ratio measurements'' obtained using all the data points on Fig. 5 from $D = 0.70$ to 4.1 mm (Chandrasekar et al. 1988; Beard et al. 1991; Kubesh and Beard 1993; present expt):

$$\alpha_A = 1.012 - 0.144D - 1.03D^2 \qquad (3)$$

with diameter units of centimeters. This second-order polynomial fit to the data has a standard deviation of $\sigma_A = 0.010$. Curve fits out to 10th order did not improve the standard deviation beyond $\sigma_A = 0.009$, because of the scatter in average axis ratios. The range of drop sizes covered by this formula should be restricted to $D = 1.1$ to about $D = 4.4$ mm. Outside this range the formula for equilibrium axis ratio [Eq. (1)] can be used, for example, for $D = 0$–1.0 mm and $D > 4.4$ mm. Removal of our two data points at $D = 2.0$ and 3.6 mm, where axisymmetric initial conditions apparently reduced the average axis ratios, did not substantially affect the above formula, because there was no perceptible difference in α_A ($\ll 0.01$) for the range $D = 1.0$–3.0 with only a 0.004 increase in α_A at $D = 4$ mm. It is not possible to capture the changes in axis ratio from $D = 1.0$ to 2.0 mm without using a fifth- (or higher) order polynomial. If such detail is needed for calculations, for example, of Z_{DR}, then we suggest using tabular values of axis ratios at 0.1-mm intervals interpolated from the mean axis ratios shown in Fig. 5. Axis ratios for $D = 0.7$–1.5 mm are given in Table 3 of Beard and Kubesh (1991).

Equation (3) for α_A should be useful for estimates of average axis ratios in rainfall where raindrop oscillations produced by raindrop collisions are a small fraction of the oscillations produced intrinsically by vortex shedding. Johnson and Beard (1984) made estimates of collision-induced oscillations that decay by viscous dissipation in exponential raindrop distributions for convective rain (Sekhon and Srivastava 1971). They found that most raindrops had oscillation energies less than 1% of the surface energy as long as their diameters were less than 4, 3.5, and 3.0 mm for rainfall rates of less than 10, 30, and 100 mm h^{-1}, respectively. The oscillation energy criterion of 1% is equivalent to an axis ratio amplitude of 0.02 for transverse mode oscillations [see Fig. 13, Beard and Kubesh (1991)], smaller than the amplitudes inferred from the data in Fig. 5. Note that the calculated contribution of drop collisions to raindrop oscillations by Johnson and Beard (1984) is overestimated because actual damping is significantly faster than for viscous dissipation (see section 4a). Therefore, Eq. (3) for α_A represents an axis ratio shift caused by raindrop oscillations that is significantly larger than that caused by drop collisions for the above limits of drop size, rainfall rates, and rainfall type.

TABLE 4. Differential reflectivities in dB for $D = 0.5$–4.5 mm using the formula of Jameson (1983) for semiempirical axis ratios (α_W; Pruppacher and Beard 1970), numerical equilibrium axis ratios (α_N; Beard and Chuang 1989), and present formula for average axis ratios of oscillating raindrops (α_{ave}). Also shown is the difference in Z_{DR} between the emperical formula of Pruppacher and Beard and the average axis ratios for oscillating raindrops: ΔZ_{DR} (dB) = Z_{DR} (α_W) − Z_{DR} (α_{ave}) and ΔZ_{DR} (%) = 100 ΔZ_{DR} (dB)/Z_{DR} (α_W).

D (mm)	Z_{DR} (α_W)	Z_{DR} (α_N)	Z_{DR} (α_{ave})	δZ_{DR} (dB)	ΔZ_{DR} (%)
0.5	0.01	0.02	—	—	—
1.0	0.33	0.16	0.13	0.20	61
1.5	0.68	0.41	0.34	0.34	50
2.0	1.00	0.76	0.60	0.40	40
2.5	1.35	1.15	0.93	0.42	31
3.0	1.71	1.61	1.34	0.37	22
3.5	2.09	2.07	1.82	0.27	13
4.0	2.48	2.54	2.38	0.10	4
4.5	2.89	3.01	—	—	—

e. Effect of raindrop oscillations on Z_{DR}

Jameson (1983) developed the following equation to evaluate the effect of changes in raindrop axis ratios on Z_{DR}:

$$Z_{DR}\ (\text{dB}) = -10.1\ \ln\langle\alpha\rangle, \tag{4}$$

where $\langle\alpha\rangle$ is the reflectivity-weighted mean axis ratio for an exponential, gamma, or Gaussian distribution of raindrop size. This equation was verified for mean axis ratios in the range from 0.66 to 0.91, corresponding to reflectivity-weighted mean drop diameters of $\langle D\rangle = 2$–6 mm. Note that raindrops larger than about 1.5-mm diameter are major contributors to Z_{DR} due to the sixth-power weighting of the drop diameter in the radar reflectivity and the increase in raindrop distortion with size.

Table 4 shows values of Z_{DR} for $\langle D\rangle = 0.5$–4.5 mm calculated from (4) using empirical axis ratios (α_W) and numerical equilibrium axis ratios (α_N), as well the average axis ratio for oscillating raindrops (α_A). Estimates of the Z_{DR} signal based on axis ratios from Pruppacher and Beard (α_W) are reduced by 0.1–0.4 dB using the average axis ratio for oscillating raindrops (α_A) in the range $\langle D\rangle = 1$–4 mm (see ΔZ_{DR}, Table 4). For small raindrops of $\langle D\rangle \approx 1$–2.0 mm, the percentage reduction in Z_{DR} is 50%–60% when using α_A instead of α_W. Goddard and Cherry (1984) proposed decreases of a few tenths dB for smaller raindrops based on observed reductions in Z_{DR} using a radar with sampling errors for Z_{DR} of order 0.1 dB in spatially uniform rain (see dashed curve in Fig. 5). According to Sachidananda and Zrnić (1987) sampling errors as low as 0.1 dB can be achieved with a 1° beamwidth S-band radar by averaging over about 100 pulses. Application to Z_{DR} is further restricted to pulse volumes uniform enough to make a useful measurement of the differential reflectivity (see Sachidananda and Zrnić 1987).

In using values of Z_{DR} to estimate reflectivity-weighted mean drop diameters from $\langle\alpha\rangle$, the axis ratio formulas can be inverted to solve for the reflectivity-weighted mean raindrop diameter for a specified $\langle\alpha\rangle$. This is illustrated in Table 5 where the drop sizes are given for the same axis ratios using the 1970 empirical formula of Pruppacher and Beard (α_W) and the present average axis ratio for oscillating raindrops (α_A). The last row is the difference in drop diameter in using these formulas at the same axis ratio, $\Delta D = D_A$ (mm) − D_W (mm). This difference in D can be verified from Fig. 5 at the same axis ratio for the plots of α_W and α_A. It represents the increase in reflectivity-weighted mean drop size for a Z_{DR} estimate of axis ratio for the present formula compared to the previous formula. Based on Table 5, inferred diameters using α_A for oscillating raindrops are about 0.1–0.6 mm larger than when using the earlier empirical formula given by Eq. (2). The biggest increases in size of 0.4–0.6 mm are for axis ratios from 0.97 to 0.84 where reflectivity-weighted mean sizes are from 1- to 3-mm diameter. Therefore, the diameter increases by about 0.5 mm when using the axis ratio formula for oscillating raindrops to interpret a measurement of Z_{DR} for a reflectivity-weighted mean drop size of less than about 3 mm.

TABLE 5. Drop diameters obtained using the 1970 empirical formula [α_W given by Eq. (2)] and the present average axis ratio for oscillating raindrops [α_A given by Eq. (3)]. The last row is the increase in drop diameter, $\Delta D = D_A$ (mm) − D_W (mm), and represents the increase in reflectivity mean drop size for Z_{DR} estimate of axis ratio in using the present formula (α_A) compared to the previous formula (α_W).

α	0.968	0.937	0.906	0.875	0.844	0.813	0.782
D_W (mm)	1.0	1.5	2.0	2.5	3.0	3.5	4.0
D_A (mm)	1.5	2.1	2.6	3.0	3.4	3.3	4.1
ΔD (mm)	0.5	0.6	0.6	0.5	0.4	0.3	0.1

6. Conclusions

Although there remains some uncertainty in utilizing raindrop axis ratios to interpret Z_{DR}, as seen by the large standard deviations in axis ratios in Fig. 5, it is readily apparent that the empirical formula (2) from Pruppacher and Beard (1970) is not the best choice to represent mean axis ratios. It is also apparent that the average axis ratios of raindrops are generally higher than the equilibrium axis ratios as represented by Eq. (1) from the numerical results of Beard and Chuang (1987), or by the hydrostatic model of Green (1975). The range for the calculations of equilibrium axis ratios, represented by the shaded region in Fig. 4, lies generally below the mean from the observations of Chandrasekar et al. (1988), Beard et al. (1989), Kubesh and Beard (1992), and the present experiment.

The formula for α_A given by Eq. (3) should be useful for estimates of average axis ratios in light to heavy rainfall where raindrop oscillations produced by raindrop collisions are a small fraction of the oscillations produced intrinsically by vortex shedding (see restric-

tions in section 5d). The size range for applying Eq. (3) for average axis ratio of raindrops is $D = 1.1$–4.4 mm. At smaller sizes, equilibrium axis ratios can be used as calculated from the Eq. (1) fit to the numerical results of Beard and Chuang (1987).

For diameters larger than about 4 mm, the axis ratio of raindrops remains uncertain. In aircraft measurements in high plains showers, Chandrasekar et al. (1988) found equilibrium axis ratios for $D = 4.1$, 4.6, and 5.1 mm. The suppression of oscillations by unmelted ice cores was suggested as a possible cause of equilibrium axis ratios. For the largest size measured ($D = 5.6$ mm) they found a large shift of 0.07 above equilibrium, but the uncertainty in the mean axis ratio was relatively large because of the limited number of measurements. Jones (1959) obtained axis ratios in heavy rainfall at the ground that were above equilibrium axis ratios by 0.13–0.20 for $D = 4$–5.6 mm. Turbulence in the surface layer may have been a factor in causing these raindrop oscillations (e.g., see Tokay and Beard 1993). The present measurement of a shift of 0.04 above equilibrium axis ratios at $D = 4.0$ mm indicates that intrinsic oscillations induced by vortex shedding may be factor in raindrop shape for sizes above 4-mm diameter. Resolution of the axis ratio for very large raindrops now awaits further measurements where the influences of drop collisions, air turbulence, and ice cores can be adequately distinguished from intrinsic oscillations caused by vortex shedding.

Acknowledgments. The authors appreciate the helpful suggestions of Dusan Zrnić and an anonymous reviewer. This material is based on work supported by the National Science Foundation under Grants ATM 91-21698, 94-21735, and 95-05298.

REFERENCES

Beard, K. V., 1976: Terminal fall velocity and shape of cloud and precipitation drops aloft. *J. Atmos. Sci.,* **33,** 851–864.

——, 1977: On the acceleration of large water drops to terminal velocity. *J. Appl. Meteor.,* **16,** 1068–1071.

——, 1983: Reorientation of hydrometeors in aircraft accelerated flow. *J. Climate Appl. Meteor.,* **22,** 1961–1963.

——, 1984: Raindrop oscillations: Evaluation of a potential flow model with gravity. *J. Atmos. Sci.,* **41,** 1765–1774.

——, and D. B. Johnson, 1984: Raindrop axial and backscatter ratios using a collisional probability model. *Geophys. Res. Lett.,* **11,** 65–68.

——, and C. Chuang, 1987: A new model for the equilibrium shape of raindrops. *J. Atmos. Sci.,* **44,** 1509–1524.

——, and A. Heymsfield, 1988: Terminal velocity adjustments for plate-like crystals and graupel. *J. Atmos. Sci.,* **45,** 3515–3518.

——, and R. J. Kubesh, 1991: Laboratory measurements of small raindrop distortion. Part II: Oscillation frequencies and modes. *J. Atmos. Sci.,* **48,** 2245–2264.

——, and A. Tokay, 1991: A field study of raindrop oscillations: Observations of size spectra and evaluation of oscillation causes. *Geophys. Res. Lett.,* **18,** 2257–2260.

——, D. B. Johnson, and A. R. Jameson, 1983: Collisional forcing of raindrop oscillations. *J. Atmos. Sci.,* **40,** 455–462.

——, H. T. Ochs, and R. J. Kubesh, 1989: Natural oscillations of small raindrops. *Nature,* **342,** 408–410.

——, R. J. Kubesh, and H. T. Ochs, 1991: Laboratory measurements of small raindrop distortion. Part I: Axis ratios and fall behavior. *J. Atmos. Sci.,* **48,** 698–710.

Bird, R. B., W. E. Stewart, and E. N. Lightfoot, 1960: *Transport Phenomena.* John Wiley and Sons, 780 pp.

Chandrasekar, V., W. A. Cooper, and V. N. Bringi, 1988: Axis ratios and oscillations of raindrops. *J. Atmos. Sci.,* **45,** 1323–1333.

Chuang, C. H., and K. V. Beard, 1990: A numerical model for the equilibrium shape of electrified raindrops. *J. Atmos. Sci.,* **47,** 1374–1389.

Goddard, J. W. F., and S. M. Cherry, 1984: The ability of dual-polarization radar (copolar linear) to predict rainfall and microwave attenuation. *Radio Sci.,* **19,** 201–208.

Green, A. W., 1975: An approximation for the shape of large raindrops. *J. Appl. Meteor.,* **14,** 1578–1583.

Jameson, A. R., 1983: Microphysical interpretation of multi-parameter radar measurements in rain. Part I: Interpretation of polarization measurements and estimation of raindrop shapes. *J. Atmos. Sci.,* **40,** 1792–1802.

——, and K. V. Beard, 1982: Raindrop axial ratios. *J. Appl. Meteor.,* **21,** 257–259.

Johnson, D. B., and K. V. Beard, 1984: Oscillation energies of colliding raindrops. *J. Atmos. Sci.,* **41,** 1235–1241.

Jones, D. M. A., 1959: The shape of raindrops. *J. Meteor.,* **16,** 504–510.

Kubesh, R. J., 1991: A laboratory investigation of raindrop oscillations. Ph.D. dissertation, University of Illinois, Champaign–Urbana, 129 pp. [Available from Dept. of Atmospheric Sciences, University of Illinois, Champaign–Urbana, 105 Gregory St., Urbana, IL 61801.]

——, and K. V. Beard, 1993: Laboratory measurements of spontaneous oscillations for moderate-size raindrops. *J. Atmos. Sci.,* **50,** 1089–1098.

List, R., and M. J. Hand, 1971: Wakes of freely falling drops. *Phys. Fluids,* **14,** 1648–1655.

Mihailovic, J., T. C. Corke, C. G. Jines, and D. R. Williams, 1997: Frequency lock-in regions for freely oscillating cylinders. *Bull. Amer. Phys. Soc.,* **42,** 2171.

Prosperetti, A., 1977: Free oscillations of drops and bubbles: The initial-value problem. *J. Fluid Mech.,* **100,** 333–347.

Pruppacher, H. R., and K. V. Beard, 1970: A wind tunnel investigation of the internal circulation and shape of water drops falling at terminal velocity in air. *Quart. J. Roy. Meteor. Soc.,* **96,** 247–256.

——, and R. L. Pitter, 1971: A semi-empirical determination of the shape of cloud and precipitation drops. *J. Atmos. Sci.,* **28,** 86–94.

——, and J. D. Klett, 1997: *Microphysics of Clouds and Precipitation.* Kluwer, 954 pp.

Sachidananda, M., and D. S. Zrnić, 1987: Rain rate estimates from differential polarization measurements. *J. Atmos. Oceanic Technol.,* **4,** 588–598.

Sekhon, R. S., and R. C. Srivastava, 1971: Doppler radar observations of drop-size distributions in a thunderstorm. *J. Atmos. Sci.,* **28,** 983–994.

Seliga, T. A., and V. N. Bringi, 1976: Potential use of radar differential reflectivity measurements at orthogonal polarizations for measuring precipitation. *J. Appl. Meteor.,* **15,** 69–76.

Tokay, A., and K. V. Beard, 1996: A field study of raindrop oscillations. Part I: Observations of size spectra and evaluation of oscillation causes. *J. Appl. Meteor.,* **35,** 1671–1687.

Winnikow, S., and B. T. Chao, 1966: Droplet motion in purified systems. *Phys. Fluids,* **9,** 50–61.

Xu, X., 1995: Analyses of aircraft measurements of raindrop shape in CaPE, M.S. thesis, Dept. of Atmospheric Sciences, University of Illinois Urbana–Champaign, 117 pp. [Available from Dept. of Atmospheric Sciences, University of Illinois, Champaign–Urbana, 105 Gregory St., Urbana, IL 61801.]